Macroscopic information-based taste representations in insular cortex are shaped by stimulus concentration

Emanuele Porcu[a,1], Karsta M. Benz[a,1], Felix Ball[a,b], Claus Tempelmann[c], Michael Hanke[a,b,d,e,2], and Toemme Noesselt[a,b,2,3]

[a]Department of Biological Psychology, Otto von Guericke University Magdeburg, 39106 Magdeburg, Germany; [b]Center for Behavioral Brain Sciences, Otto von Guericke University Magdeburg, 39106 Magdeburg, Germany; [c]Department of Neurology, Otto von Guericke University Magdeburg, 39120 Magdeburg, Germany; [d]Brain & Behaviour (INM-7), Institute of Neuroscience and Medicine, Research Centre Jülich, 52425 Jülich, Germany; and [e]Institute of Systems Neuroscience, Medical Faculty, Heinrich Heine University Düsseldorf, 40225 Düsseldorf, Germany

Edited by Linda M. Bartoshuk, University of Florida, Gainesville, FL, and approved February 21, 2020 (received for review October 1, 2019)

Taste processing is an essential ability in all animals signaling potential harm or benefit of ingestive behavior. However, current evidence for cortical taste representations remains contradictory. To address this issue, high-resolution functional MRI (fMRI) and multivariate pattern analysis were used to characterize taste-related informational content in human insular cortex, which contains primary gustatory cortex. Human participants judged pleasantness and intensity of low- and high-concentration tastes (salty, sweet, sour, and bitter) in two fMRI experiments on two different days to test for task- and concentration-invariant taste representations. We observed patterns of fMRI activity within insular cortex narrowly tuned to specific tastants consistently across tasks in all participants. Fewer patterns responded to more than one taste category. Importantly, changes in taste concentration altered the spatial layout of putative taste-specific patterns with distinct, almost nonoverlapping patterns for each taste category at different concentration levels. Together, our results point at macroscopic representations in human insular cortex as a complex function of taste category and concentration rather than representations based solely on taste identity.

gustatory | human | fMRI | MVPA | concentration

In mammals, taste identification constitutes a critical ability to ensure survival through selection of nutritional vs. potentially harmful food. Although humans have developed a fine ability to distinguish different tastes and taste compounds, it is yet unclear how basic and mixed tastes are distinctively represented in the gustatory cortex (GC).

Other sensory cortices are traditionally characterized by specific topological organizations of neurons arranged into specialized functional maps (e.g., orientation maps in the primary visual cortex or tonotopic maps in the primary auditory cortex). Hence, one might hypothesize that there is a functional map type of organization (1) in chemosensory cortices as well, based on basic taste categories. Yet, it still needs to be proven whether any general topological principle applies to gustatory cortices (see ref. 2 for olfaction).

Only recently have putative gustotopic maps been observed in rodents (e.g., ref. 3). There, pools of neurons were characterized by direct associations with specific taste qualities (salty, sweet, bitter, and umami) within specialized subregions of mouse's insular cortex. In clear contradistinction, however, the majority of animal studies reported overlapping clusters of neurons broadly tuned to distinct tastes (e.g., ref. 4; for review see ref. 5). For instance, Fletcher et al. (6) showed that neurons were preferentially tuned to specific tastes or combination of tastes; nonetheless, such neurons were intermingled with neurons tuned to different tastes, in line with the notion of a nontopological gustatory organization in other species (for similar results in nonhuman primates see, e.g., ref. 7).

In humans, to date, the organization of the GC remains poorly understood. The putative human GC, located in anterior to middle insula (8, 9), is inherently a multisensory area (10, 11) which exhibits a wide range of responses not exclusively related to gustatory stimuli (e.g., somatosensory and thermal responses). This organization makes it particularly challenging to isolate activity elicited by taste stimuli from other influences (e.g., somatosensory responses).

In accord with the vast majority of animal data, most population-based* human imaging studies—though operating on a coarser spatial scale than single-cell studies and two-photon-imaging, which prevent direct comparability—have reported a scattered organization of activated clusters broadly tuned to different taste categories, with no actual evidence of dedicated taste-specific maps (e.g., ref. 12). Only a few functional MRI (fMRI) studies (13, 14) have reported taste-specific clusters of voxels which may resemble a gustotopic type of organization. However, both studies were penalized by small sample sizes, passive tasting (i.e., lack of task), and constant intensity per taste. The latter two points strongly limit the generalizability of these findings as intensity variations can dramatically alter macroscopic responses to tastes (12, 15, 16), as can the task at hand (17, 18). Moreover,

Significance

Previous research has produced mixed results concerning cortical representations of taste categories. The main objective of the present study was to test for task- and concentration-invariant maps in human insular cortex through an information-based approach. We tested identical participants in two functional MRI (fMRI) experiments on different days and successfully decoded patterns of fMRI activity associated with each specific taste category in all participants across distinct behavioral tasks and time, suggesting robust task-invariant taste representations in all individual participants. Most importantly, low- and high-concentration taste-preferring representations showed very little overlap, contradicting the notion of an exclusively topological organization in insular cortex based only on taste identity.

Author contributions: M.H. and T.N. designed research; E.P. and K.M.B. performed research; E.P. and K.M.B. analyzed data; and E.P., K.M.B., F.B., C.T., M.H., and T.N. wrote the paper.

The authors declare no competing interest.

This article is a PNAS Direct Submission.

Data deposition: The datasets/code supporting the current study have been deposited in Open Science Framework (https://osf.io/2m5sk/).

[1]E.P. and K.M.B. contributed equally to this work.

[2]M.H. and T.N. contributed equally to this work.

[3]To whom correspondence may be addressed. Email: toemme@med.ovgu.de.

This article contains supporting information online at https://www.pnas.org/lookup/suppl/doi:10.1073/pnas.1916329117/-/DCSupplemental.

First published March 16, 2020.

*The term "population-based," though common in the imaging literature, may evoke unintended associations with the labeled-line vs. population-coding debate. In this paper the term "macroscopic" will be used instead to prevent misunderstandings.

previous studies have relied exclusively on mass-univariate analyses, whereby a statistical model is fit to each voxel independently, thus failing to capture information uniquely carried by patterns of activity across neighboring voxels. To overcome this impasse, Crouzet et al. (19) used a multivariate approach with electrophysiological data to explore the temporal profile of taste processing; more recently, Chikazoe et al. (20) adopted a multivariate approach to classify patterns of fMRI signals to basic taste categories as well as different chemical compounds of the same taste categories. While these authors were able to identify common patterns of activities in the insular cortex associated with basic taste qualities, irrespective of chemical compounds, the lack of variation in tastant concentration and task compromises the conclusion that a taste-specific map indeed exists. Moreover, the absence of an adequate measure to quantify the selectivity of specific patterns for particular taste categories further impairs their interpretation. Hence, the aim of the present study was to test for a general gustotopic organization and, more specifically, to provide a comprehensive characterization of the human GC as a function of 1) taste quality (bitter, salty, sweet, or sour), 2) taste concentration (high or low), and 3) task (pleasantness and intensity judgments). To this end, 24 participants were tested in two fMRI experiments in which we administered four basic taste categories at two different concentrations plus an additional neutral compound. Participants judged intensity in one experiment and pleasantness in the other experiment. Crucially, a spatially constrained classifier (searchlight approach) was trained on data of the first experiment and tested on the second experiment, and vice versa, to identify common, task-independent yet taste-specific representations. Moreover, taste-specific tuning functions were calculated for each searchlight to address the issue of narrow vs. wide taste-specific tuning functions in human insular cortex. Finally, across- and within-concentration classification analyses were used to assess the influence of concentration on taste-specific representations.

Results

Behavior. Participants were able to correctly perceive taste identity in the majority of all cases (*SI Appendix*, Fig. S1 *A* and *B*). Moreover, they rated taste valence differently depending on taste concentration and taste identity, as testified by the significant interaction [$F(4, 23) = 3.028$, $P = 0.0186$; $\eta^2 = 0.030$], with sweet always showing significantly enhanced and bitter showing significantly decreased ratings compared to neutral (see *SI Appendix*, Table S1 and Fig. S1*C* for details). Concerning the intensity judgments, participants perceived a consistent difference in intensity between high and low concentrations, as expected [main effect of intensity: $F(1, 23) = 34.398$, $P < 0.001$; $\eta^2 = 0.181$]. Moreover, a main effect of taste identity was observed [$F(4, 23) = 9.810$, $P < 0.001$; $\eta^2 = 0.280$], while the interaction between intensity and taste identity did not reach significance [$F(4, 23) = 2.237$, $P > 0.05$; $\eta^2 = 0.048$; see *SI Appendix*, Table S1 and Fig. S1*D* for details].

Neural Underpinnings. The central focus of this study was to characterize the functional organization of putative GC, and thus left and right insular cortex were targeted by means of regions of interest (ROIs) derived from independent functional parcellation of the insula (21). Since the exact location of human GC is still debated (see, e.g., ref. 8), several definitions of human GC within subfields of the insula have been proposed (e.g., refs. 21 and 22) which are not always consistent. Therefore, we placed additional results based on different human GC definitions in *SI Appendix*, Figs. S2 and S3 and Tables S2 and S3 but show the unbiased results covering the whole insula (which contains GC) in the main text. Moreover, we overlaid the subfields which may contain human GC based on combined resting-state , diffusion-tensor imaging, and functional labeling results (21) on the functional results (see yellow outlines in Figs. 1 and 4 and see *SI Appendix*, Figs. S2 and S3 for another definition of GC [note again that below we report results for the whole insula to avoid unduly biasing the results]).

Sparse multinomial logistic regression (23) was used to train and test, in turn, on the first experiment and second experiment through a searchlight approach (24).

Cross-Experiment Decoding. First, we isolated fMRI patterns associated with taste categories. Given previous reports on the influence of taste concentration on fMRI signals (e.g., ref. 16), separate classifications were calculated for high and low intensities. These critical comparisons will unveil task-invariant yet single or multiple taste-preferring patterns if present.

High concentration. Classification among high-concentration tastes revealed patterns of spheres for all four taste categories which were successfully decoded across the two experiments (Fig. 1*A*, *Right*). For this analysis, we first estimated probabilities (rather than accuracies) to quantify the selectivity of each searchlight sphere for a given taste quality. This set of probabilities provides a continuous multidimensional measure describing the selectivity of each searchlight sphere (one probability for each taste) rather than a "winner-take-all" accuracy measure (25). After initial classification, we then estimated evidence ratios (ERs) by contrasting correct classifications with false positives (i.e., higher probability of a particular taste when another taste was presented; see Fig. 1*A* for significant ER maps, p[cluster] < 0.05, familywise error rate [FWE]-corrected, with an auxiliary threshold of p[voxel] < 0.001). Statistical maps of ER were subsequently used to assess the selectivity of each sphere, based on a tuning index. In particular, tuning indices (range 0 to 1) were computed based on the ER for a particular taste relative to the highest evidence for all other tastes. Indices larger than 0.5 indicate an increasingly narrow tuning for a specific taste category (see *Methods* for further details). Together, our results provide evidence for a consistent narrow selectivity for all taste categories across experiments, that is, independent of task (see Fig. 1*B* for tuning maps).

Moreover, the number of spheres narrowly tuned to one particular taste varied, with bitter showing consistent effects in ∼4.3% of insular spheres and salty in ∼3.5% of insular spheres, while sweet and sour registered ∼2.8% and ∼1.8%, respectively. Similar sphere counts were obtained in both left and right insula. Next, we tested for spheres broadly tuned to more than one taste. However, virtually none of the clusters coding a combination of two or three tastes survived the selection criteria.

To confirm at the single-subject level that these sphere-based observations are not simply due to large interindividual differences in topologies due to group-mean voxel-based averaging (13, 14), we next tested for differential effects of taste category based on single-subject results (see Fig. 1*C* for tuning maps of an illustrative subject). Here, 8.89% (median ± 1.2% SE), 8.40% ± 1.2%, 8.38% ± 1.2%, and 6.75% ± 1.1% of insular spheres averaged over hemispheres responded to salty, bitter, sweet, and sour, respectively (see Fig. 2*A*, top column for scatter plots of all individual taste categories; see also *SI Appendix*, Fig. S2, second row and *SI Appendix*, Tables S2 and S3, top).

All subjects expressed taste-selective spheres for all tastants (see *SI Appendix*, Table S4, top). No significant differences in sphere count were observed for hemisphere, taste category, or their interaction (*P*s = 0.4 and higher), mirroring the group-level results (although note that subject-specific sphere counts are higher than group-level counts, indicating increased sensitivity). Moreover, the number of spheres was not related to perceived intensity or pleasantness for any taste ($P \geq 0.424$, Bonferroni-corrected). Finally, lower counts were found for two-taste–(0.5% ± 0.3%) and three-taste–preferring spheres (see Fig. 2*A*, middle and bottom columns); more than half of the subjects did

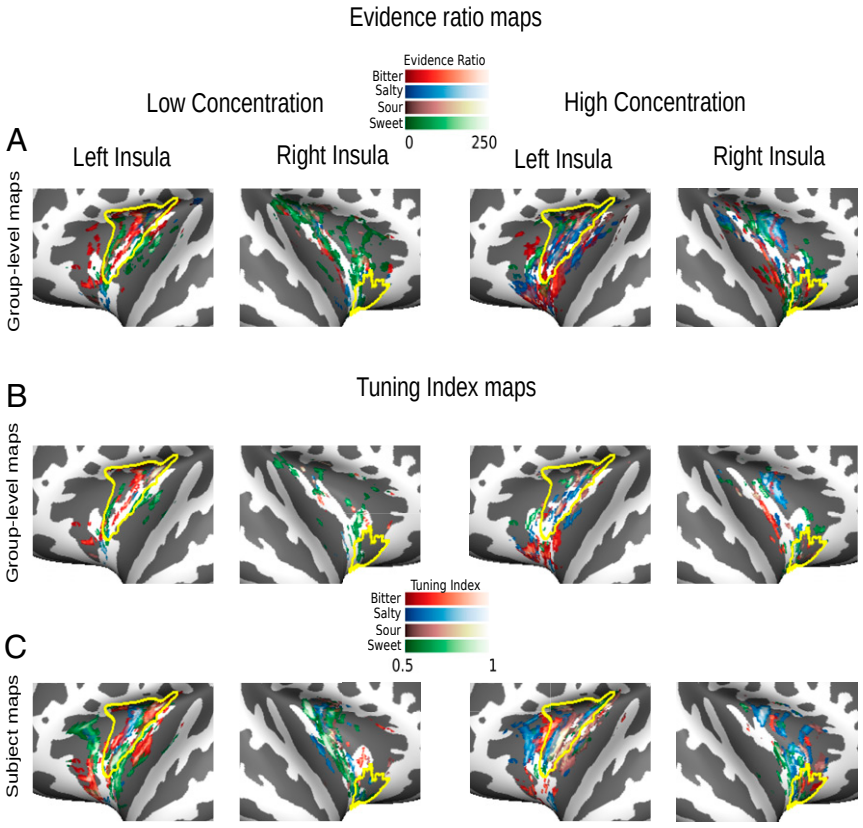

Fig. 1. Cross-experiment taste maps. (*A*) Flat maps depict significant clusters of ERs (cluster-thresholded at p_{FWE} <0.05 with an auxiliary voxel threshold of $P <$ 0.001) in insular cortex at the group level, obtained through cross-experiment decoding. Plots were created by projecting three-dimensional brain voxels onto a two-dimensional surface via Nilearn 0.5.0 (40) and subsequently plotting the brain surfaces by using Visbrain 0.4.0 (45). Note that ERs for particular tastes can and do overlap as ERs represent reliability of our classification independently for each taste category. (*B*) Tuning maps depict spheres narrowly tuned to single tastes at the group level (thresholded at >0.5). (*C*) Tuning maps for an illustrative subject. The information provided by group-level maps may be misleading given the extreme variability of the insula's functional microstructure (13, 14). Single-subject maps exhibit a stronger degree of spatial continuity for specific taste categories than the group-level maps. Left columns always represent low concentration tastes, and right columns represent high concentration tastes. Yellow lines depict GC as defined by Fan et al. (21); see *SI Appendix*, Figs. S2 and S3 for further information.

not show any significant three-taste–preferring clusters (see also *SI Appendix*, Table S4). No significant differences across hemispheres or taste category were observed for the double or triple-tuned spheres, confirming the pattern observed at the group level. When further restricting the analysis to putative GC within the insula (*SI Appendix*, Fig. S2) the number of subjects exhibiting spheres tuned to two tastes dropped drastically compared to the analysis of the whole insula, whereas spheres tuned to single tastes were found in all (*SI Appendix*, Table S3, top) or more than 87% of all subjects (*SI Appendix*, Table S2, top) depending on the exact definition of GC. In contrast, ∼45% of subjects did on average not show any spheres tuned to two tastes and over 85% did not show any response to three tastes in any sphere (*SI Appendix*, Tables S2 and S3).

Low concentration. As a second critical comparison, we tested for task-invariant taste-specific patterns at low concentration. Fig. 1*A*, *Left* depicts significant clusters of ER maps for each taste category for the low-concentration stimuli. As for high-concentration maps, we again observed task-invariant yet taste-selective clusters for all four tastes (Fig. 1*B*). Overall cluster sizes were comparable to those observed for the high-concentration conditions at the group level. In particular, the subjects-specific sphere count for the low-concentration conditions revealed an increase in insular spheres tuned to sweet (∼4.7%), while bitter (∼2.3%), salty (∼0.7%), and sour (∼1.5%) preferences slightly decreased relative to high-concentration spheres. As for the high concentration, virtually none of the clusters were tuned to more than one taste category. Again, confirmatory analyses of single-subject results corroborated the group-level results (Fig. 2*B*), with higher counts for single-taste–preferring spheres (bitter: 8.27% ± 1.0; salty: 6.88% ± 0.9; sour: 7.47% ± 1.0; sweet: 9.68% ± 1.3) than two- and three-taste–preferring spheres (see also *SI Appendix*, Table S4).

Moreover, subjective intensity or pleasantness ratings were again not related to subject-specific sphere counts for any taste category ($P \geq 0.512$, Bonferroni-corrected). Together, the findings for both concentration levels reveal that there are consistent taste-preference clusters in the insula and that most taste-sensitive spheres expressed a preferential tuning to one taste only. As observed for high concentration, when restricting the analysis to putative GC the number of participants exhibiting spheres tuned to two tastes dropped drastically compared to the whole insula, whereas spheres tuned to single tastes were found in ∼96% (*SI Appendix*, Table S3, top) or more than 93% of all subjects (*SI Appendix*, Table S2, top) depending on the exact definition of GC. In contrast, ∼46% (or over 50% depending on the exact definition of GC) of the subjects did on average not show spheres tuned to two tastes and ∼90% did not show any response to three tastes in any sphere (*SI Appendix*, Tables S2 and S3).

However, these analyses above were independent from each other and thus cannot answer the critical question of whether the observed task-independent taste-specific subregions were also independent of taste concentration.

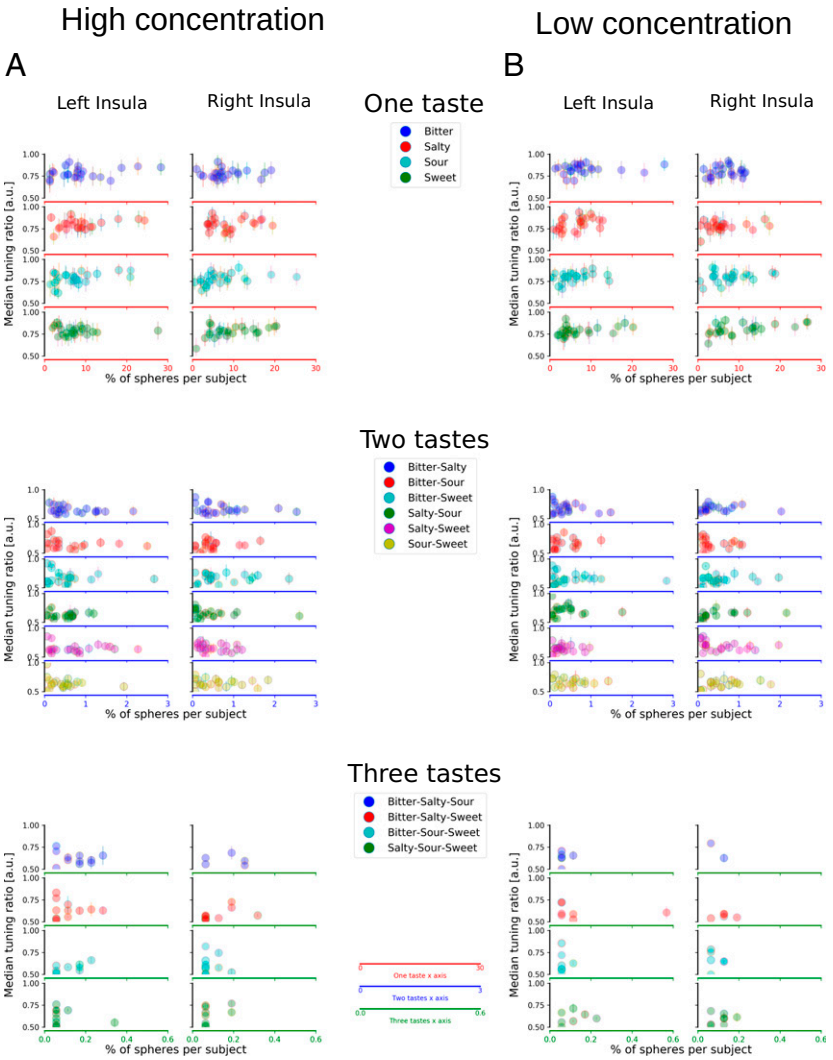

Fig. 2. Subject-specific TIs. Scatter plots depict median TIs for all subjects (each dot represents a subject) separately for high (*A*) and low (*B*) concentrations in insular cortex (see *SI Appendix*, Figs. S2 and S3 for gustatory ROIs). The *y* axis represents the median TIs for a specific taste or a compound of tastes. A TI of 0.75 indicates that the ER for the preferred taste was three times higher than the second-highest ER (see *Methods* for further details). The *x* axis indicates the percentage of spheres which show a preferential tuning for a taste or a compound of tastes. Scatter plots, from top to bottom, represent percentage of spheres tuned to single tastes (two top columns), double tastes (two middle columns), and triple tastes (two bottom columns); the left and right columns of each taste configuration represent the left and right insula, respectively. Note that the *x* axis is scaled differently for single-, double- and triple-taste spheres (top, middle, and bottom columns) due to the decreasing number of spheres responsive to double- and triple-taste compounds.

High vs. Low Concentrations. The most critical comparison therefore tested whether the observed task-independent clusters were also not affected by stimulus concentration. For this direct fine-grained analysis of the relationship between high and low concentration maps, we quantified the amount of overlap between high- and low-concentration maps for both group and single-subjects maps for all taste categories. Specifically, we counted the number of spheres coactive in low- and high-concentration tuning maps and we then computed the ratio between the number of coactive spheres using geometric mean between the two compared cluster sizes. Geometric averaging was adopted to account for the overall different size of the clusters of interest. Otherwise, the chance to observe high or low overlap might have been biased by the relative size of each cluster (e.g., two bigger clusters would have had a higher probability to share common spheres than two small clusters). This procedure provided a continuous index of overlap ranging between 0 and 1, where 0 indicates no overlap and 1 indicates complete overlap. We computed the index of overlap separately for each taste to determine to which extent spheres that showed a preference for a specific taste at a low concentration showed a preference for the same or a different taste at a high concentration. The overlap between high- and low-concentration maps—obtained from the cross-experiment classification—were extremely low, suggesting distinct taste-related patterns as a function of stimulus intensity (see Fig. 3*A* middle diagonal, bitter left insula: 0, bitter right insula: 0, salty left insula: 0.03, salty right insula: 0, sour left insula: 0.05, sour right insula: 0, sweet left insula: 0, sweet right insula: 0.04; see *SI Appendix*, Fig. S4 for virtually identical results at the single-subject level and also *SI Appendix*, Fig. S5, where we explore further response characteristics of coactive spheres). In addition, some spheres even switched their taste-specific preference (e.g., from bitter to sour as indicated by the off-diagonal cells), yet no regularities could be observed in the switching patterns (although note that the number of overlapping spheres was relatively low).

Finally, we tested whether the few concentration-invariant spheres anatomically group together in a particular region of the

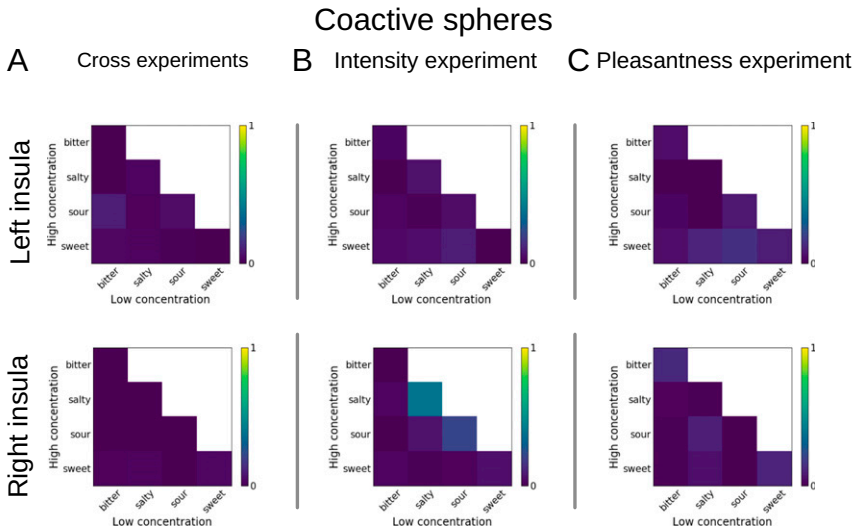

Fig. 3. Coactive spheres across taste concentrations. (*A*) Heat maps depict the coactivity index of spheres based on data from narrowly tuned spheres for the cross-experiment decoding. Coactivity is expressed as an index of overlapping spheres across concentrations, where 0 indicates the absence of overlap and 1 complete overlap. (*B*) Heat maps represent the coactivity index based on classifications for intensity judgments. (*C*) Heat maps represent the coactivity index for pleasantness judgments. The main diagonal represents coactive spheres coding for the identical taste category across concentrations. Values outside the main diagonal indicate a switch in taste preference as a function of concentration.

insula. Since the insula contains many higher-order gustatory and multisensory regions in addition to the primary GC (PGC), we reasoned that concentration-invariant spheres might be clustered in PGC. To test this, we first generated group-mean maps for each taste. However, no location of insula contained concentration-invariant spheres from more than three participants. Second, we checked whether any particular subfield within the insula contained most of the subject-specific concentration-invariant spheres using the subfield definition provided by Fan et al. (21) including all six subfields regardless of their putative functional properties. However, concentration-invariant spheres were present in all subfields but were usually found in less than half of all participants per subfield (*SI Appendix*, Fig. S6). Thus, we observed no anatomical hotspot for concentration-invariant spheres.

Within-Experiments Decoding. In order to further confirm that the topological distinction observed between low and high concentrations was consistent in each single experiment and not merely due to task differences across the two experiments, we performed four additional classifications (i.e., we separately decoded high and low concentrations within each experiment). For this analysis, the cross-validation was based on a different training and test set: A leave-one-out procedure was used in which the classifier was trained on three out of the four runs and tested on the remaining one. As expected, we were again able to decode patterns of spheres, here within the individual experiments, which were associated with each taste at high and low concentrations (Fig. 4 *A* and *B*). In Fig. 3 *B* and *C* we show the index of overlap between high and low concentrations separately for each experiment; as for the cross-experiments maps (see Fig. 3*A*), we see very little overlap between high- and low-concentration maps in the within-experiment analyses.

Cross-Concentrations Decoding. Finally, in order to confirm whether high- and low-concentration maps reflect truly distinct macroscopic representations, we performed two additional classifications, one per experiment. We trained the classifier on the low-concentration tastes and tested on the high-concentration tastes, and vice versa, for each experimental session.

We reasoned that if different spheres are coding for low and high concentrations, we should observe a poor classification. In line with our hypothesis and the previous decoding results, we indeed observed only a small amount of spheres coding indiscriminately for low- or high-concentration tastes (Fig. 4*C*): Based on the tuning maps, in experiment 1, bitter exhibits only 0.1% of narrowly tuned spheres, salty 0.5%, sour 0.15%, and sweet 0.17%; similar results were obtained in experiment 2, where bitter exhibits 1.2%, salty 0.15%, sour 0.5%, and sweet 0.4%. Together, this pattern of results is in clear disagreement with the notion of broad concentration-invariant maps of taste qualities in the human insula.

Discussion

The main objective of the present study was to test for task- and concentration-invariant maps in human GC through an information-based approach. We tested identical participants in two distinct fMRI experiments on different days and successfully decoded patterns of spheres associated with each specific taste category in all participants across distinct behavioral tasks and time, suggesting robust task-invariant taste representations in all individual participants. Most importantly, low- and high-concentration taste-selective representations showed very little overlap, contradicting the notion of an exclusively topological organization based on linguistic taste labels.

Significantly extending previous observations (20), we observed patterns narrowly, but not exclusively, tuned to specific tastes as well as patterns of more broadly tuned spheres in the left and right insula at the group level and confirmed taste-specific patterns when considering only one concentration. The information provided by group-level maps may nonetheless misrepresent the actual organization observable at the single-subject level given the extreme variability of the insula's functional microstructure, as previously pointed out (13, 14). When inspecting single-subjects' maps, we observed patterns exhibiting a stronger degree of spatial continuity for specific taste categories. It has to be noted, though, that such subject-specific tuning maps showed a mixture of spheres narrowly tuned toward one taste category and others exhibiting a broader tuning while keeping a distinct preference for a specific taste.

As a consequence of the structural variability across individuals, spheres equally tuned to two or three tastes were virtually absent at the group level. Also, at the single-subject level, the

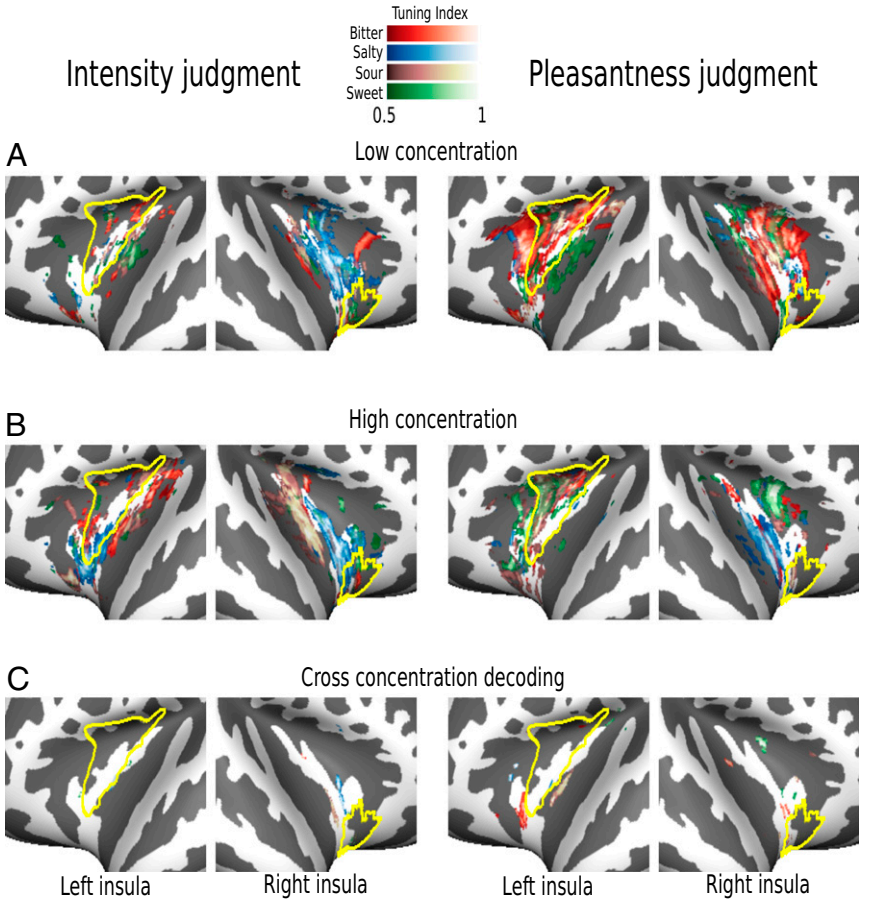

Fig. 4. Within-experiments tuning maps. (*A*) Flat maps depict narrowly tuned spheres in insular cortex for low-concentration tastes, separately for intensity judgments (*Left*) and pleasantness judgments (*Right*). (*B*) Maps depict narrowly tuned spheres in insular cortex for high-concentration stimuli, for intensity (*Left*) and pleasantness (*Right*) judgments, respectively. (*C*) Plots depict maps representing tuning indices for cross-concentrations decoding for each taste category, separately for intensity (*Left*) and pleasantness (*Right*) judgments. Note that within concentration decoding produces consistent results (*A* and *B*), whereas cross-concentration decoding (*C*) reveals almost no consistent clustering. Yellow lines depict GC as defined by Fan et al. (21); see *SI Appendix*, Figs. S2 and S3 for further information.

number of spheres coding two tastes was much smaller than spheres coding single tastes (Fig. 2) and were further reduced when restricting the analysis to GC; likewise, only a few subjects showed spheres coding for three different tastes and almost none showed spheres with these response properties in GC. This lack of patterns equally tuned to different tastes might be ascribed to the stringent criteria that we adopted to identify tuning indices. Alternatively, responses in multitaste spheres might be more easily elicited by presenting compound tastes, which was not part of our current experimental design. In line with our results, however, Fletcher et al. (6) also observed single taste preferences in the majority of neurons.

Considering topological theories, we do not find any evidence for common maps across concentrations, although stable patterns were observed for single concentrations, in line with previous research (3, 13). Crucially, we observed a patchy organization in insular cortex for different taste categories rather than a highly ordered topography (3, 13). Thus, our data support a model of distributed patterns of activity coding for different taste qualities rather than a model of highly specialized maps on the macroscopic level. In particular, a distributed model seems to be supported by the distinct topological organization that we observed in high- and in low-concentration maps (note that even for the low-concentration tastes all behavioral responses differed from each other, pointing to a sufficiently high concentration for perception, in accord with the distinct patterns of neural activity). Especially at the single-subject level (*SI Appendix*, Fig. S4), small subsets of the spheres that preferentially coded for a specific taste at low concentration changed their preference to a different taste at high concentration, hence suggesting that taste coding might dynamically change according to relevant features and might be achieved through distributed representations rather than rely exclusively on rigid functional maps on the macroscopic level. Indeed, while only a small number of concentration-independent taste-preferring spheres were found in our study, concentration-dependent taste-preferring spheres were more common and found in all participants. However, the exact spatial layout differed between participants and did not seem to follow a highly organized topological arrangement.

One might argue that the difference in representation of low- vs. high-concentration tastes might be due to the fact that participants were less able to identify the low-concentration tastes (relative to the higher ones). However, a confusion between different low-concentration tastes should lead to less-stable decoding patterns rather than the stable patterns for each low-concentration taste observed here. Moreover, the lack of overlap for low- and high-concentration patterns also suggests that the coding mechanisms in the GC differs from other, topologically ordered systems (e.g., vision): There, a change in stimulus intensity may modulate the firing rate of identical neurons and

classification accuracy (due to changes in signal-to-noise ratio) yet should yield similar overall patterns, whereas with our gustatory results tuning patterns stay robust (Fig. 2) but seem to change location. In accord, a recent study conducted in mice (26) targeted sensory neurons in the geniculate ganglion, hence focused on an earlier stage of taste processing, and found a robust change in preferential tuning when taste concentration was systematically varied. Up to 51% of the narrowly tuned neurons exhibited a taste-selectivity change from narrow to broad tuning, suggesting that at least at an intermediate processing stage mice brains rely on a pattern-coding mechanism.

Finally, the amount of overlapping spheres between high- and low-concentration maps was consistently low. In some cases, there were no overlapping spheres, thus suggesting that, at least partially, two different underlying populations of neurons might be preferentially coding for a taste category at high and low concentrations. Our observations are also supported by a recent study in rats (27), which shows that over a large number of neurons only a "small" subset is able to code for both high and low concentrations of sucrose. In accord, a monkey study (28) observed that less than 1.5% of the recorded neurons in the insular cortex exhibited a linear response as a function of the increase in glucose concentration. Although those studies report effects on the cellular level and might thus be difficult to directly link to macroscopic fMRI results, it has nevertheless been shown for the visual modality that orientation tuning can be picked up with fMRI (29), even though the spatial resolution of fMRI was much coarser than the size of orientation columns. Potentially, a similar effect was observed here.

In previous human and animal studies, changes in concentration have shown seemingly contradictory scenarios. On the one hand, an increase in concentration led to monotonic increase in activations (e.g., ref. 4), firing rate (e.g., ref. 28), and event-related potential amplitudes (e.g., refs. 15 and 30). On the other hand, several studies have shown complex nonlinear behaviors: High concentrations led to decrease in firing rate or responses uniquely triggered by intermediate concentrations (e.g., refs. 31 and 32). A recent univariate fMRI study by Canna et al. (16) reported a nonlinear relation between blood oxygen level–dependent response and concentration, with a reduction in fMRI signals for middle and high concentrations. Our findings are in line with the latter observation. A plausible model of the neural underpinnings would either require a group of generalist neurons responsive to multiple classes of tastes and different ranges of concentrations, or alternatively a group of specialized intermingled neurons, each tuned to specific tastes and concentrations, although note that these two models are not mutually exclusive (28, 31) and that our fMRI measure is on the macro scale. Alternatively, changes in concentration could already affect peripheral coding of tastes, with enhanced cross-talk between particular receptors at higher concentrations (e.g., bitter and salty; see ref. 33). Although we did observe random changes in taste selectivity with our macroscopic measure, these effects might still contribute to our concentration-dependent effects. In addition to these more physiological mechanisms which could in principle account for the different patterns observed for high and low concentrations a fourth alternative explanation could be based on the coding of psychological factors such as palatability and hedonic values (e.g., ref. 34). As shown by human and animal electrophysiology (see ref. 35 for review), taste detection, discrimination (17), and concentration modulate very early components, but palatability might reflect later components (36), although recently Wallroth and Ohla (17) have suggested early modulation of hedonic features. Thus, given that our activations are convolved over an extremely long time window, the effects that we are observing in low and high concentrations might be caused by differences in palatability.

Thus, the organizational principle in GC could be based on valence rather than physical stimulus properties. In contrast to this notion, the largest taste-specific effects found here were task-independent and did not vary with perceived pleasantness (or intensity). Hence, we propose that the variation in neural signaling—which was linked to valence in previous human imaging studies (13, 18)—may rather be based on changes of a physical property (i.e., concentration) which governs perceived pleasantness and significantly shapes informational content in low-level GC.

In summary, our results demonstrate patterns in the human insular cortex preferentially tuned to specific taste categories in all single subjects plus some more broadly tuned patterns. Importantly, variations in stimulus concentration reveal complex changes of activity with little overlap between concentration-dependent taste-specific representations. Together, these results point at a distributed type of organization in GC with local taste preferences on the macroscopic level and highlight that GC might be coding a complex mixture of taste identity and concentration rather than a representation based solely on taste identity.

Methods

Participants. Twenty-five healthy volunteers took part in two experiments; one participant was excluded from the final analysis due to a technical problem with taste delivery, hence resulting in 24 participants (16 female, age: mean = 24.9 y, SD = 3.6). Participants fulfilled the following inclusion criteria: no known allergies/sensitivity to the chemical solutions used in the experiments, no respiratory tract infections in the 2 wk prior to the experiments, no neurological and psychiatric disorders, no ongoing diets, no regular intake of medication, no smokers. Additionally, participants were asked to abstain from ingesting any food or caloric drink within the 3 h prior to the experiments. In order to assess normal tasting and smelling abilities, participants passed two clinical tests: Taste Stripes and Sniffin' Sticks (Burghart Messtechnik). The study protocol was approved by the local ethics committee of the Otto von Guericke University Magdeburg and all participants gave written informed consent.

Stimuli. We used four distinct tastants (bitter, salty, sour, and sweet) plus a neutral solution (artificial saliva). Solutions were provided by the central pharmacy of the medical faculty of Otto von Guericke University Magdeburg. Stimuli were obtained from the following basis solutions (= 100%): 600 mM NaCl (salty), 1 M glucose (sweet), 0.1 mM quinine hydrochloride (bitter), and 8 mM citric acid (sour). The neutral solution consisted of 5 mM KCl and 0.5 mM $NaHCO_3$, the same chemical compounds as saliva (37), though at lower concentration as O'Doherty et al. (37) based on own piloting. With the exception of the neutral taste, all stimuli were presented at two different concentrations (low and high), which were chosen via pilot testing in order to guarantee a discernible difference between the two concentrations. The resulting stimuli were obtained according to the following percentages of basis solution dissolved with pure water (low/high): 10%/70% salty, 20%/80% sweet, 20%/100% bitter, and 10%/80% sour.

Stimuli were delivered through an automated stimulation device: Gustometer GU002 (Burghart Messtechnik). The Gustometer allows the control of stimulus duration and concentration and massively reduces undesirable somatosensory stimulation given that stimuli are sprayed via compressed air directly onto the tip of the participants' tongues. The Gustometer delivers the stimulus at *ca*. 40 °C, resulting in approximately the body temperature of the stimulus upon tongue contact. The device was controlled through MATLAB 2012b (MathWorks, Inc.) via custom-made scripts and Psychophysics Toolbox (38) running on a Windows 7 environment.

Stimuli were delivered to the participant through a pump held by a custom-made Plexiglas scaffolding mounted above the head coil. Participants were asked to protrude the tip of their tongue and enclose it with their lips in order to prevent to ingest the liquid. None of the participants reported any physical discomfort related to this procedure. The liquid was then absorbed by a tissue placed below the participant's mouth. This procedure was adopted to avoid any motion- and swallowing-related artifacts and most importantly to isolate taste-related activity while avoiding or holding constant other confounding factors (e.g., temperature, stimulation of oral cavity, etc.).

Experimental Procedure. Participants took part in two scanning sessions with a minimum time interval of 1 d and a maximum of 7 mo. Before and after the

two scanning sessions participants—while lying in the scanner—were asked to identify taste stimuli by choosing among five options presented on the screen (bitter, neutral, salty, sour, and sweet) after each taste delivery, resulting in four distinct identifications per taste category in total (see *SI Appendix*, Fig. S1 *A* and *B* for descriptive results).

The main experiment consisted of four runs, each composed of 45 trials. Each run consisted of sequences of stimuli comprised of all tastes in both concentrations plus the neutral taste. All sequences had to fulfill three basic constraints: 1) Each stimulus was presented five times within each run, 2) the same stimulus could never be presented twice in a row, and 3) each combination of two consecutive stimuli was presented at least once during the entire experiment by using De Brujin sequences.

During scanning, each trial started by concurrently displaying the word "Schmecken" ("Taste" in German) and spraying the tastant on the tongue of the participant. The stimulation consisted of four distinct sprays (250 ms each) interspersed with four pauses (250 ms each) for a total duration of 2 s; each spray released 50 μL of tastant, summing up to a total of 200 μL per trial. The tastant delivery was followed by a rating scale which assessed intensity or pleasantness for the first and second experiment, respectively ("Wie intensiv/angenehm empfinden Sie diesen Geschmack?", "How intense/pleasant does this taste?" in German). Participants were asked to provide their rating on a 9-point scale ranging from 1: "No perception" to 9: "Extremely intense" or "Extremely unpleasant" to "Extremely pleasant" displayed on the screen. In order to respond, participants slid a green cursor through the numbers of the scale by pressing two buttons with the index and middle finger of the right hand. To confirm their choice, participants pressed a third button with the thumb. For each rating scale, the green cursor was randomly located on a different digit upon scale display to avoid biasing. In case a participant was unable to provide an answer within 6 s after the appearance of the scale, the response was considered invalid. Immediately after the rating scale, the word "Rinse" was presented on the screen together with 2 s of sprayed water to rinse the tongue from the previous tastant. The following trial started after an intertrial interval of 2 s (total trial duration 12 s).

Neuroimaging Data Collection. Scanning was conducted on a Siemens Prisma 3 Tesla system with a 32-channel head coil for signal reception. T_1-weighted structural images were acquired with an MPRAGE sequence using the following parameters: $1 \times 1 \times 1$ mm^3 voxel size, $256 \times 256 \times 192$ matrix, 2.82-ms echo time, 2.5-s repetition time, 1.1-s inversion time, 7° flip angle, 140-Hz per pixel bandwidth, 7/8 partial Fourier, parallel imaging with a GRAPPA factor of 2, and 5:18-min scan duration.

For functional imaging we opted for a combination of reduced field-of-view (rFOV) gradient echo planar imaging (EPI) and parallel imaging in order to minimize signal dropout and geometric distortion. This technique is part of the Siemens "Advanced fMRI" work-in-progress software. During each of the four functional runs we acquired 280 volumes using the following parameters: 24 slices, 1.8-mm slice thickness, 0.9-mm interslice gap, ascending slice excitation order, 135- × 240-mm^2 rFOV, 1.25- × 1.25-mm^2 in-plane voxel size, 30-ms echo time, 2-s repetition time, 90° flip angle, 1 mT/m·ms z-shim, 0.73-ms echo spacing, and GRAPPA factor of 2. The transversal slice block was tilted 20° with respect to the anterior commissure–posterior commissure line.

To facilitate the registration and normalization of the rFOV we additionally acquired 10 whole-brain EPI volumes. In order to keep geometrical distortions within the rFOV part of the whole-brain dataset identical to the functional scans the shim settings were copied and the FOV and matrix size in phase direction as well as the GRAPPA factor were doubled. A Siemens autoalign algorithm was used to automatically select the identical slices during the second scanning session.

Data Analysis

Behavioral Data. Ratings of intensity and pleasantness were analyzed with the same statistical procedure: We first computed the median across all of the ratings separately for each experimental condition. Each dataset was then subjected to a repeated-measures ANOVA with the factors taste category (bitter, salty, sour, sweet, and neutral) and intensity (high and low). Post hoc *t* tests were subsequently performed to statistically test potential differences among taste ratings. In order to correct for multiple comparisons, Bonferroni correction was applied.

Brain–behavior correlations were computed using Pearson's correlation coefficients and Bonferroni corrections. Effects of taste category and intensity were analyzed using repeated measures ANOVAs with the factors hemisphere and taste category, separately for low and high concentrations. All analyses were performed by using the R package stats v3.6.0 within the R environment (v3.4.4).

fMRI Data Preprocessing. fMRI analysis was conducted within a computational cluster in a Debian environment; analysis tools were obtained through NeuroDebian (39).

Both datasets were subject to the identical preprocessing procedure: Prior to any preprocessing, four dummy scans collected at the beginning of each scanning session were removed from each dataset. Motion correction was performed by realigning, each volume of both experiments to the first volume of experiment 1 via a rigid body transformation (MCFLIRT, FSL 5.09).

For noise reduction, time series were temporally filtered by means of a band-pass filter (cutoffs: 4 Hz and 150 Hz). Additionally, each volume was spatially smoothed by applying a full width at half maximum Gaussian kernel of 4 mm via Nilearn 0.5.0 (40).

Multivariate Pattern Analysis. Decoding analysis was performed with PyMVPA (41) and custom Python scripts. Prior to the multivariate pattern analysis (MVPA), each time series was fitted on a voxel-by-voxel basis with a general linear model (GLM) using Nipy 0.4.2 (42).

The GLM was composed of five "taste" regressors (neutral, bitter, salty, sour, and sweet; trial onset aligned with start of taste delivery, duration 2 s) convolved with a canonical hemodynamic response function with temporal derivatives. Motion estimates (six degrees of freedom) were included as additional nuisance regressors. In order to subtract potential artifacts common to each taste condition, GLM parameters for each taste were contrasted runwise against the neutral condition and the resulting t-contrasts were used as features for classification.

We then applied a sparse multinomial logistic regression classifier (SMLR) (23) and a leave-one-out cross-validation procedure. The type of folding used for cross-validation changed according to the aim of the specific classification performed. For the cross-experiment classification, the SMLR was, in turn, trained on one experiment and tested on the other one; for the cross-concentration classification, the SLMR was trained on low-concentration data and tested on the high-concentration data, and vice versa. For the within-experiment classifications (separate classifications for high and low concentrations for both experiments), the SMLR was, in turn, trained on three out four runs and tested on the remaining run. Classification was restricted to voxels in the insula using the brain parcellation provided by Fan et al. (21), with a 50% cutoff criterion for the probability maps. Insular ROIs included the following left and right subregions: dorsal dysgranular insular (dId), dorsal agranular insular (dIa), ventral agranular insular (vIa), dorsal granular insular (dIg), ventral granular insular (vIg/vId), and hypergranular insular (G) cortex.

Decoding was performed through a searchlight approach (24) with a sphere's radius of four voxels. The primary outcome of the classification analysis were the taste-categorywise probability estimates of the SMLR classifier, for each searchlight sphere and each data fold.

MVPA Statistical Analysis. In order to assess the degree of evidence for a response to a specific presented taste, we computed the following ratio for each taste and searchlight sphere:

$$PE(T) = med(P(T))$$

for each taste category across all data folds.

$$ER(T) = \frac{PE(T)}{max(PE(\sim T))},$$

where $PE(T)$ denotes the median of the SMLR probability estimates $P(T)$ for one specific taste across all trials in which this particular taste was presented. $PE(\sim T)$ is the median of probability estimates for the same taste based across all trials in which this particular taste was not presented (i.e., a different taste was presented). The rationale adopted for the ER resembles the concept of the Bayes factor, by comparing the alternative $PE(T)$ and null $PE(\sim T)$ hypothesis to assess the goodness of the model of interest.

ER computation yields a single map for each taste. In total, four ERs, one for each taste, were calculated per data fold. Importantly, if two tastes independently express a consistent and high probability for a given sphere, both of them will have a high ER, and thus ER does not bias the results toward narrow tuning. ERs simply provide a necessary metric to ensure the reliability of our classification independently for each test. The obtained maps were then statistically evaluated at the group level following a bootstrapped permutation analysis proposed by Stelzer et al. (43), implemented in PyMVPA, and briefly summarized here: In order to assess the null distribution of results, we computed 50 additional "chance" result maps for each participant, using the identical analysis setup and data folding strategy, while permuting the taste labels within the training data. For group-level inference, all individual maps were spatially transformed and resliced, via

FSL FLIRT, from native image space into Montreal Neurological Institute space with a 2-mm isotropic voxel size.

The empirical group-average map was thresholded using a variable voxelwise cutoff, corresponding to $P < 0.001$ of the distribution of results from 10,000 bootstrap samples of group average maps, computed from randomly drawn "chance" maps, one for each participant. Likewise, group-level cluster size was statistically tested ($P < 0.05$) based on the distribution of cluster sizes across the 10,000 bootstrap samples, after applying the same $P < 0.001$ voxelwise threshold to all "chance" group average maps.

Quantifying Tuning Maps. In order to quantify the degree of selectivity for each taste or a combination of taste categories, we computed an index of preferential tuning for each sphere. Tuning indices (TIs) were based on ERs and calculated by using the single-taste ERs (e.g., salty) or by combining the ERs of different tastes (e.g., bitter and salty). Importantly, TIs were calculated both on the group level and single subjects' statistical maps according to the following equation:

$$TI(T) = \frac{min(ER(T))}{max(ER(T)) + max(ER(\sim T))},$$

where $ER(T)$ indicates the ER for a single taste or a combination of tastes of interest and $ER(\sim T)$ indicates the ERs of the remaining tastes. In case of single taste tuning, $min(ER(T))$ and $max(ER(T))$ are simply $ER(T)$. The choice of taking the minimum of ER(T)—in the numerator—and maximum of $ER(T)$—in the denominator—becomes relevant only when we want to evaluate the selectivity of a combination of tastes (e.g., bitter and salty). Selecting the smaller $ER(T)$ in the numerator and the bigger $ER(T)$ in the denominator prevents that two highly different ER values would produce a TI above 0.5, which would indeed provide a misleading characterization of that sphere's preference. TIs guarantee that a given sphere can be considered as preferentially tuned to a taste or a combination of tastes only if the TI is bigger than 0.5. Hence, they provide a rather conservative measure (range 0 to 1) either in favor—values above 0.5—or not in favor of the selected taste—values below 0.5. Note that TIs of 0.75 (the average value across subjects; see Fig. 2 and *SI Appendix*, Figs. S2 and S3) indicate that the highest ER was three times higher than the second-highest ER. Additionally, to avoid selecting extremely low but significant ERs, we selected spheres with $ER(T)$ equal or larger than 3 for at least one taste. This threshold was motivated by the analogy with the Bayes factor, where values equal or larger than 3 are considered indicative of a moderate evidence (44). While this thresholding ensures the identification of spheres reliably tuned to a particular taste and thus diminishes the chance of false positives, it may sometimes lead to abrupt changes in TIs within a sphere. However, lowering the ER threshold level to 2.5 did not lead to a significant increase in coactive voxels within the same test category.

Data/Code Availability. The datasets/code supporting the current study have been deposited in a public repository (https://osf.io/2m5sk/).

ACKNOWLEDGMENTS. E.P., F.B., M.H., and T.N. were funded by a grant provided by the Deutsche Forschungsgemeinschaft: DFG-SFB779/TPA15.

1. S. P. Wilson, J. A. Bednar, What, if anything, are topological maps for? *Dev. Neurobiol.* **75**, 667–681 (2015).
2. A. J. Giessel, S. R. Datta, Olfactory maps, circuits and computations. *Curr. Opin. Neurobiol.* **24**, 120–132 (2014).
3. X. Chen, M. Gabitto, Y. Peng, N. J. P. Ryba, C. S. Zuker, A gustotopic map of taste qualities in the mammalian brain. *Science* **333**, 1262–1266 (2011).
4. R. Accolla, B. Bathellier, C. C. H. Petersen, A. Carleton, Differential spatial representation of taste modalities in the rat gustatory cortex. *J. Neurosci.* **27**, 1396–1404 (2007).
5. D. B. Katz, M. A. L. Nicolelis, S. A. Simon, Gustatory processing is dynamic and distributed. *Curr. Opin. Neurobiol.* **12**, 448–454 (2002).
6. M. L. Fletcher, M. C. Ogg, L. Lu, R. J. Ogg, J. D. Boughter, Jr, Overlapping representation of primary tastes in a defined region of the gustatory cortex. *J. Neurosci.* **37**, 7595–7605 (2017).
7. T. R. Scott, C. R. Plata-Salamán, Taste in the monkey cortex. *Physiol. Behav.* **67**, 489–511 (1999).
8. E. Iannilli, N. Noennig, T. Hummel, A. M. Schoenfeld, Spatio-temporal correlates of taste processing in the human primary gustatory cortex. *Neuroscience* **273**, 92–99 (2014).
9. M. G. Veldhuizen *et al*., Identification of human gustatory cortex by activation likelihood estimation. *Hum. Brain Mapp.* **32**, 2256–2266 (2011).
10. T. Hanamori, T. Kunitake, K. Kato, H. Kannan, Responses of neurons in the insular cortex to gustatory, visceral, and nociceptive stimuli in rats. *J. Neurophysiol.* **79**, 2535–2545 (1998).
11. N. Gogolla, The insular cortex. *Curr. Biol.* **27**, R580–R586 (2017).
12. D. M. Small *et al*., Dissociation of neural representation of intensity and affective valuation in human gustation. *Neuron* **39**, 701–711 (2003).
13. A. Prinster *et al*., Cortical representation of different taste modalities on the gustatory cortex: A pilot study. *PLoS One* **12**, e0190164 (2017).
14. M. A. Schoenfeld *et al*., Functional magnetic resonance tomography correlates of taste perception in the human primary taste cortex. *Neuroscience* **127**, 347–353 (2004).
15. K. Ohla, U. Toepel, J. le Coutre, J. Hudry, Electrical neuroimaging reveals intensity-dependent activation of human cortical gustatory and somatosensory areas by electric taste. *Biol. Psychol.* **85**, 446–455 (2010).
16. A. Canna *et al*., Intensity-related distribution of sweet and bitter taste fMRI responses in the insular cortex. *Hum. Brain Mapp.* **40**, 3631–3646 (2019).
17. R. Wallroth, K. Ohla, As soon as you taste it: Evidence for sequential and parallel processing of gustatory information. *eNeuro* **5**, ENEURO.0269-18.2018 (2018).
18. F. Grabenhorst, E. T. Rolls, A. Bilderbeck, How cognition modulates affective responses to taste and flavor: Top-down influences on the orbitofrontal and pregenual cingulate cortices. *Cereb. Cortex* **18**, 1549–1559 (2008).
19. S. M. Crouzet, N. A. Busch, K. Ohla, Taste quality decoding parallels taste sensations. *Curr. Biol.* **25**, 890–896 (2015).
20. J. Chikazoe, D. H. Lee, N. Kriegeskorte, A. K. Anderson, Distinct representations of basic taste qualities in human gustatory cortex. *Nat. Commun.* **10**, 1048 (2019).
21. L. Fan *et al*., The human Brainnetome Atlas: A new brain atlas based on connectional architecture. *Cereb. Cortex* **26**, 3508–3526 (2016).
22. T. Yarkoni, R. A. Poldrack, T. E. Nichols, D. C. Van Essen, T. D. Wager, Large-scale automated synthesis of human functional neuroimaging data. *Nat. Methods* **8**, 665–670 (2011).
23. B. Krishnapuram, L. Carin, M. A. T. Figueiredo, A. J. Hartemink, Sparse multinomial logistic regression: Fast algorithms and generalization bounds. *IEEE Trans. Pattern Anal. Mach. Intell.* **27**, 957–968 (2005).
24. N. Kriegeskorte, R. Goebel, P. Bandettini, Information-based functional brain mapping. *Proc. Natl. Acad. Sci. U.S.A.* **103**, 3863–3868 (2006).
25. S. Anzellotti, M. N. Coutanche, Beyond functional connectivity: Investigating networks of multivariate representations. *Trends Cogn. Sci.* **22**, 258–269 (2018).
26. A. Wu, G. Dvoryanchikov, E. Pereira, N. Chaudhari, S. D. Roper, Breadth of tuning in taste afferent neurons varies with stimulus strength. *Nat. Commun.* **6**, 8171 (2015).
27. E. Fonseca, V. de Lafuente, S. A. Simon, R. Gutierrez, Sucrose intensity coding and decision-making in rat gustatory cortices. *eLife* **7**, e41152 (2018).
28. T. R. Scott, C. R. Plata-Salaman, V. L. Smith, B. K. Giza, Gustatory neural coding in the monkey cortex: Stimulus intensity. *J. Neurophysiol.* **65**, 76–86 (1991).
29. Y. Kamitani, F. Tong, Decoding the visual and subjective contents of the human brain. *Nat. Neurosci.* **8**, 679–685 (2005).
30. H. Tzieropoulos, A. Rytz, J. Hudry, J. le Coutre, Dietary fat induces sustained reward response in the human brain without primary taste cortex discrimination. *Front. Hum. Neurosci.* **7**, 36 (2013).
31. J. R. Stapleton, M. L. Lavine, R. L. Wolpert, M. A. L. Nicolelis, S. A. Simon, Rapid taste responses in the gustatory cortex during licking. *J. Neurosci.* **26**, 4126–4138 (2006).
32. C. J. MacDonald, W. H. Meck, S. A. Simon, Distinct neural ensembles in the rat gustatory cortex encode salt and water tastes. *J. Physiol.* **590**, 3169–3184 (2012).
33. Y. Oka, M. Butnaru, L. von Buchholtz, N. J. P. Ryba, C. S. Zuker, High salt recruits aversive taste pathways. *Nature* **494**, 472–475 (2013).
34. R. Accolla, A. Carleton, Internal body state influences topographical plasticity of sensory representations in the rat gustatory cortex. *Proc. Natl. Acad. Sci. U.S.A.* **105**, 4010–4015 (2008).
35. K. Ohla *et al*., Recognizing taste: Coding patterns along the neural axis in mammals. *Chem. Senses* **44**, 237–247 (2019).
36. B. F. Sadacca, J. T. Rothwax, D. B. Katz, Sodium concentration coding gives way to evaluative coding in cortex and amygdala. *J. Neurosci.* **32**, 9999–10011 (2012).
37. J. O'Doherty, E. T. Rolls, S. Francis, R. Bowtell, F. McGlone, Representation of pleasant and aversive taste in the human brain. *J. Neurophysiol.* **85**, 1315–1321 (2001).
38. D. H. Brainard, The psychophysics toolbox. *Spat. Vis.* **10**, 433–436 (1997).
39. Y. O. Halchenko, M. Hanke, Open is not enough. Let's take the next step: An integrated, community-driven computing platform for neuroscience. *Front. Neuroinform.* **6**, 22 (2012).
40. A. Abraham *et al*., Machine learning for neuroimaging with scikit-learn. *Front. Neuroinformatics* **8**, 14 (2014).
41. M. Hanke *et al*., PyMVPA: A python toolbox for multivariate pattern analysis of fMRI data. *Neuroinformatics* **7**, 37–53 (2009).
42. K. J. Millman, M. Brett, Analysis of functional magnetic resonance imaging in Python. *Comput. Sci. Eng.* **9**, 52–55 (2007).
43. J. Stelzer, Y. Chen, R. Turner, Statistical inference and multiple testing correction in classification-based multi-voxel pattern analysis (MVPA): Random permutations and cluster size control. *Neuroimage* **65**, 69–82 (2013).
44. R. E. Kass, A. E. Raftery, Bayes factors. *J. Am. Stat. Assoc.* **90**, 773–795 (1995).
45. E. Combrisson *et al*., Sleep: An open-source Python software for visualization, analysis, and staging of sleep data. *Front. Neuroinform.* **11**, 60 (2017).